

Muon to positron conversion

MyeongJae Lee ^{1,†}  and Michael MacKenzie ^{2,†,‡} 

¹ Center for Axion and Precision Physics research, Institute for Basic Science, Daejeon 34051, Republic of Korea; myeongjaelee@ibs.re.kr

² Northwestern University, Evanston, Illinois, 60208, USA; michaelmackenzie@u.northwestern.edu

* Correspondence: michaelmackenzie@u.northwestern.edu

† These authors contributed equally to this work.

‡ Corresponding author.

Abstract: Lepton flavor violation (LFV) has been discovered in the neutrino sector by neutrino oscillation experiments. The minimally extended Standard Model (SM) to include neutrino masses allows LFV in the charged sector (CLFV) at the loop-level, but at rates that are too small to be experimentally observed. Lepton number violation (LNV) is explicitly forbidden even in the minimally extended SM, where the observation of a LNV process would be unambiguous evidence of physics beyond the SM. The search for the LNV and CLFV process $\mu^- + N(A, Z) \rightarrow e^+ + N'(A, Z - 2)$ (referred to as $\mu^- \rightarrow e^+$ conversion) is a complementary LNV channel to $0\nu\beta\beta$ decay searches, sensitive to potential flavor effects in the neutrino mass generation mechanism. A theoretical motivation for $\mu^- \rightarrow e^+$ conversion is presented along with a review of the status of past $\mu^- \rightarrow e^+$ conversion experiments and future prospects. Special attention is taken to understanding an uncertain and potentially dominant background for these searches, radiative muon capture, and its potential impacts on current and future $\mu^- \rightarrow e^+$ searches.

Keywords: Muon; muon conversion; charged lepton flavor violation; CLFV; lepton number violation; LNV

1. Introduction

The incoherent conversion of a negative muon into a positron in a muonic atom, $\mu^- + N(A, Z) \rightarrow e^+ + N'(A, Z - 2)$ (referred to as $\mu^- \rightarrow e^+$ hereafter), is an exotic rare process that is both lepton flavor violating (LFV) and lepton number violating (LNV) with a change in lepton number by two units ($\Delta L = 2$). In the Standard Model (SM), there is no explicit symmetry corresponding to lepton flavor conservation, however its conservation has been empirically established, for example in muon or tau lepton decays. The LFV decay of the muon has been studied experimentally in the last few decades in three major processes: $\mu^+ \rightarrow e^+\gamma$, $\mu^+ \rightarrow e^+e^-e^+$, and $\mu^- + N \rightarrow e^- + N$ (referred to as $\mu^- \rightarrow e^-$). The most recent result on muon LFV processes comes from the MEG experiment searching for $\mu^+ \rightarrow e^+\gamma$, presenting $B(\mu^+ \rightarrow e^+\gamma) < 4.2 \times 10^{-13}$ with 90% confidence level (C.L.) [1]. The upgrade of the MEG experiment to improve the experimental sensitivity by 10 times up to 6×10^{-14} is in progress [2], and is expected to begin data acquisition very soon. The Mu3e [3] experiment is the next generation experiment of $\mu^+ \rightarrow e^+e^-e^+$ searches at PSI, and for $\mu^- \rightarrow e^-$, new results with 100 - 10,000 times better sensitivity are expected during 2020s from the COMET [4] and Mu2e [5] experiments.

The theoretical branching ratio expectations for muon LFV decays in the SM are extremely small, on the order of 10^{-54} , as the rate is suppressed by $(m_\nu/M_W)^4$ where m_ν is the neutrino mass and M_W is the W-boson mass [6]. Therefore, the observation of such a LFV process is regarded as direct evidence of physics beyond the SM. The tau LFV measurements from B-factory experiments and the LHCb experiment have been yielding impressive progress [7], but only reaching the $\mathcal{O}(\sim 10^{-7} - 10^{-8})$ upper limit level, mainly because of the difficulty in producing a large number of tau lepton pairs in the case of the B-factory experiments.



Citation: Muon to positron conversion. *Preprints* 2021, 1, 0. <https://doi.org/>

Received:

Accepted:

Published:

Publisher's Note: MDPI stays neutral with regard to jurisdictional claims in published maps and institutional affiliations.

In the LNV case, such a process is not allowed as a perturbative process. The minimal extension of the SM with a Majorana neutrino assumption allows for the famous LNV process, neutrinoless double-beta decay ($0\nu\beta\beta$), to occur. In fact, $\mu^- \rightarrow e^+$ is very similar to $0\nu\beta\beta$, as depicted in Figure 1, except that $\mu^- \rightarrow e^+$ is also affected by a lepton flavor change. Benefiting from the progress in detector technology and the feasibility of obtaining a large amount of target material, LNV can be studied best with $0\nu\beta\beta$. This is in progress at many experiments, such as KamLAND-Zen [8] as the most recent resulting example. The $\mu^- \rightarrow e^+$ process is a complementary study to $0\nu\beta\beta$, as LNV may be enhanced in $\mu^- \rightarrow e^+$ over $0\nu\beta\beta$, which may imply that the effect from the flavor off-diagonal sectors ($e\mu$ or $e\tau$) manifest the LNV, while the diagonal component (ee) can be suppressed in some theories. The LNV effect of $0\nu\beta\beta$ is more dominating than the $\mu^- \rightarrow e^+$ in the case that a light Majorana neutrino mediates the LNV, but the effect of, for example, a heavy sterile neutrino is not very well studied. A possible difference between $\mu^- \rightarrow e^+$ and $0\nu\beta\beta$ was suggested by some theories beyond the SM [9–15]. In addition, some theories explain the LNV of $0\nu\beta\beta$ without a Majorana neutrino exchange, but instead using a new mediator particle from a supersymmetric theory or a Majoron: see the discussion by Engel and Menéndez [16] and the references therein. These new physics models beyond the SM are also applicable to explain the possible existence of $\mu^- \rightarrow e^+$. Therefore, from one perspective, $\mu^- \rightarrow e^+$ is a LNV search mediated by a Majorana neutrino similar to $0\nu\beta\beta$ experiments, and from another perspective, it is a new physics search regarding the flavor effect on the neutrino mixing in the framework of the theory beyond the SM. While there are other LNV searches such as $\tau^- \rightarrow e^+\pi^-\pi^-$ [17] or $K^\pm \rightarrow \pi^\mp\mu^\pm\mu^\pm$ [18], those are not similar processes to $0\nu\beta\beta$ or $\mu^- \rightarrow e^+$, so they cannot be directly compared.

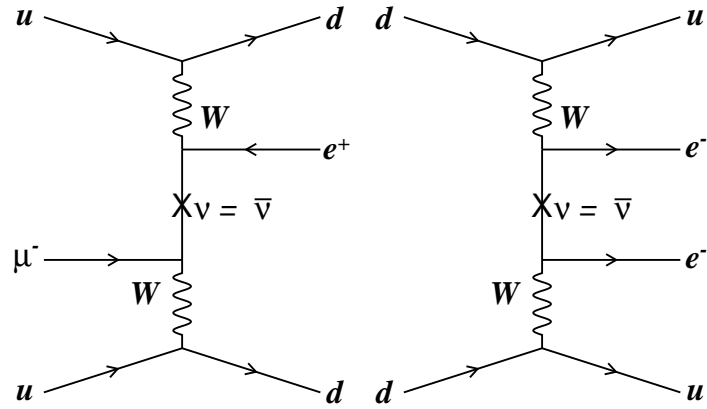


Figure 1. The tree level diagram of $\mu^- \rightarrow e^+$ (left) and $0\nu\beta\beta$ (right) in a Majorana neutrino model.

From the experimental point of view, $\mu^- \rightarrow e^+$ is attracting more interest as the future $\mu^- \rightarrow e^-$ experiments progress. The COMET [4] and Mu2e [5] experiments will search for $\mu^- \rightarrow e^-$ up to the order of 10^{-17} in sensitivity. The $\mu^- \rightarrow e^+$ signal can be easily distinguished from $\mu^- \rightarrow e^-$ by the charge identification. Although those experiments are not optimized for $\mu^- \rightarrow e^+$ in terms of the target material selection and beamline design, it is obvious that the sensitivity reach of $\mu^- \rightarrow e^+$ searches can be significantly improved at the future COMET and Mu2e $\mu^- \rightarrow e^-$ experiments. The current best experimental limits on $\mu^- \rightarrow e^+$ were obtained by the SINDRUM II collaboration with titanium nuclei: $B(\mu^- + \text{Ti} \rightarrow e^+ + \text{Ca}) < 1.7 \times 10^{-12}$ with 90% C.L. to the ground state of calcium [19].

The objective of this article is to emphasize the physical importance of the $\mu^- \rightarrow e^+$ search and describe its feasibility in future $\mu^- \rightarrow e^-$ experiments. Section 2 reviews the

theoretical and experimental status of $\mu^- \rightarrow e^+$, and Section 3 describes a mitigation strategy for suppressing the background in $\mu^- \rightarrow e^+$ searches at future $\mu^- \rightarrow e^-$ experiments.

2. Theories and past results

2.1. Estimation of the $\mu^- \rightarrow e^+$ conversion rate in the extended SM with a Majorana neutrino

A generic model of the neutrino mass includes at least three light, left-handed neutrinos, with the neutrino flavor oscillation described by the Pontecorvo–Maki–Nakagawa–Sakata (PMNS) matrix. A right-handed neutrino, or any other hypothetical neutrino, may have significantly larger mass than the light neutrinos. This is expected, for example, from the Seesaw mechanism. In the minimal extension of the SM, the $\mu^- \rightarrow e^+$ process is allowed through a light or heavy Majorana neutrino exchange, as depicted in Figure 1. But, as described before, it is also possible that other new particles beyond the SM or new interactions between quarks and leptons may mediate the interaction.

Assuming the light or heavy Majorana neutrino exchange interaction, the leading order $\mu^- \rightarrow e^+$ matrix element when the initial and final states of nuclei are both ground states can be written as [20]:

$$\begin{aligned} \mathcal{M}_{fi} &= -i \left(\frac{G_F}{\sqrt{2}} \right)^2 \frac{1}{(2\pi)^{3/2}} \frac{1}{\sqrt{4E_{\mu^-} E_{e^+}}} \bar{v}(k_{e^+}) (1 + \gamma_5) u(k_{\mu^-}) \\ &\quad \times \frac{m_e g_A^2}{2\pi R} \left[\frac{\langle m_\nu \rangle_{\mu e}}{m_e} \mathcal{M}_\nu + \langle M_N^{-1} \rangle_{\mu e} m_p \mathcal{M}_N \right] \times 2\pi \delta(E_{\mu^-} + E_i - E_f - E_{e^+}) \quad (1) \\ &\propto \begin{cases} \langle m_\nu \rangle_{\mu e} \mathcal{M}_\nu & \text{(light neutrino)} \\ \langle M_N^{-1} \rangle_{\mu e} \mathcal{M}_N & \text{(heavy neutrino)} \end{cases} \end{aligned}$$

In this equation, G_F is the Fermi constant, m_e is the electron mass, g_A is the weak axial coupling constant, and R is the nuclear radius. $E_{(\mu^-, e^+, f, i)}$ represent the energy of the muon, positron, final nuclear ground state, and initial nuclear ground state, respectively. The effective neutrino masses are defined as:

$$\langle m \rangle_{\alpha\beta} = \sum_k U_{\alpha k} U_{\beta k} m_k, \quad (2)$$

for the light neutrino, and

$$\langle M_N^{-1} \rangle_{\alpha\beta} = \sum_k \frac{U_{\alpha k} U_{\beta k}}{M_k}, \quad (3)$$

for the heavy neutrino. α and β are flavor indexes, and m_k and M_k represent the light neutrino mass and the heavy neutrino mass, respectively. U is the neutrino mixing matrix, or PMNS matrix for the light neutrino case. The effective neutrino mass matrix can be calculated from the current estimation of the neutrino masses and mixing angles, in the case of the light neutrino exchange model. For example, from a cosmological observation, the sum of three light neutrino masses is less than 0.42 eV, which translates to $\langle m_\nu \rangle_{l_1 l_2} < 0.14$ eV [21].

Another important term in Equation 1 is $\mathcal{M}_{\nu/N}$, representing the nuclear matrix element (NME) for the light and heavy neutrino, respectively. This is a transition probability matrix of the nucleon from the initial state to the final state:

$$\mathcal{M}_i \propto \int dq \sum_n \langle f | J^\mu(x) | n \rangle \langle n | J^\nu(y) | i \rangle = \mathcal{M}_i^{(GT)} + \mathcal{M}_i^{(T)} + \mathcal{M}_i^{(F)}, \quad (4)$$

where n is the intermediate state and q and J represent the momentum transfer and hadronic current, respectively. Theoretically, it is divided into three components: the axial vector

($\mathcal{M}_i^{(GT)}$, Gamow-Teller term), tensor ($\mathcal{M}_i^{(T)}$), and vector ($\mathcal{M}_i^{(F)}$, Fermi term) components, where the axial vector NME is the dominant effect [16,22]. Because of uncertainties in the nucleus models, and difficulty of calculating many body dynamics, the calculation of NME usually requires moderate methods of approximation: see the reviews by Vergados et al. [23] and Engel and Menéndez [16] for approximation methods of NME calculation used for $0\nu\beta\beta$ experiments, such as the interacting shell model (ISM), quasiparticle random-phase approximation (QRPA), interacting boson model (IBM), projected Hartree-Fock-Bogoliubov model (PHFB), and energy density functional method (EDF). Engel and Menéndez [16] also describe that the NME calculations of various target materials for $0\nu\beta\beta$ changes by up to a factor of three, which implies the importance of theoretical understanding of NME in studying the $\mu^- \rightarrow e^+$ process in the minimal extension of the SM with a Majorana neutrino.

Using this formulation, the theoretical estimation of the $\mu^- \rightarrow e^+$ rate was obtained by Domin et al. [20]:

$$\begin{aligned} \mathcal{R}^{\mu^- e^+} &\equiv \frac{\Gamma(\mu^- + N(A, Z) \rightarrow e^+ + N'(A, Z - 2))}{\Gamma(\mu^- + N(A, Z) \rightarrow (\text{All muon captures}))} \\ &= 2.6 \times 10^{-22} \times \left\{ \begin{array}{l} |\langle m_\nu \rangle_{\mu e} / m_e|^2 |\mathcal{M}_\nu|^2 \quad (\text{light neutrino}) \\ |\langle M_N^{-1} \rangle_{\mu e m_p}|^2 |\mathcal{M}_N|^2 \quad (\text{heavy neutrino}) \end{array} \right\} \end{aligned} \quad (5)$$

Applying the effective neutrino mass obtained from the experimental data on the neutrinos mass and mixing, and the NME for titanium from the QRPA method, $\mathcal{R}^{\mu^- e^+}$ (Ti) is:

$$\begin{aligned} &(0.008 - 1.7) \times 10^{-41} \quad \text{for a light neutrino, normal neutrino mass hierarchy,} \\ &(0.05 - 6.7) \times 10^{-40} \quad \text{for a light neutrino, inverted neutrino mass hierarchy, and} \\ &\leq 3.8 \times 10^{-24} \quad \text{for a heavy neutrino.} \end{aligned}$$

While the estimated $\mu^- \rightarrow e^+$ rate is much higher in the heavy Majorana neutrino case than the light neutrino one, it is far smaller than the feasible experimental reach. While the search for $\mu^- \rightarrow e^+$ may not affect the understanding of the sterile or Majorana neutrino, it would imply that any observation above the expected conversion rate would lead necessitate a theory beyond the minimal extension of the SM with a massive Majorana neutrino.

Any $\Delta L = 2$ interaction other than the tree level interaction depicted in Figure 1 may lead to $\mu^- \rightarrow e^+$. This possibility was studied by Berryman et al. [9] by using an effective operator description and normalizing the estimation of the Majorana neutrino exchange case (including one and two loop corrections) with the above tree-level calculation. The conversion rate was estimated according to the energy scale of the new physics (Λ), where the result is shown in Figure 2. From the sensitivity limit of Mu2e, the new physics energy scale accessible from a $\mu^- \rightarrow e^+$ measurement is comparably low, around 40 GeV. For all possible $\Delta L = 2$ interactions leading to $\mu^- \rightarrow e^+$ and $0\nu\beta\beta$, the new physics scale reach of $\mu^- \rightarrow e^+$ is a few orders of magnitude smaller than $0\nu\beta\beta$ experiments. Quoting the conclusion by Berryman et al. [9], under this theoretical estimation, the observation of $\mu^- \rightarrow e^+$ will lead to conclusions that: the neutrino is a Majorana fermion, flavor effects suppress $0\nu\beta\beta$ while enhancing $\mu^- \rightarrow e^+$, and a combination of complex interactions other than the tree-level interaction is responsible for the physics of nonzero neutrino mass.

Table 1. The $\mu^- \rightarrow e^+$ experimental results so far [24]. The upper limits are at the 90 % C.L. N_{capture} is the number of muon captures in the experiments. GS and GRE represent ground state and giant resonance excitation of the final nucleus status. While the ^{32}S and ^{127}I are almost 100 % in natural abundance among their isotopes, Ti and Cu are not, which is the reason for not specifying the mass of Ti and Cu.

| Nuclei | Upper limit | N_{capture} | Year | Experiment | Detector | GS/GRE | Reference |
|------------------|-----------------------|----------------------|------|------------|---------------|--------|-----------|
| Ti | 3.6×10^{-11} | 2.5×10^{13} | 1998 | SINDRUM-II | Drift chamber | GRE | [19,26] |
| | 1.7×10^{-12} | | | | | GS | |
| | 8.9×10^{-11} | 4.9×10^{12} | 1993 | SINDRUM-II | Drift chamber | GRE | [27] |
| | 4.3×10^{-12} | | | | | GS | |
| | 1.7×10^{-10} | 9×10^{12} | 1988 | (TRIUMF) | TPC | GRE | [28] |
| ^{32}S | 9×10^{-10} | 6.7×10^{11} | 1980 | SIN | Calorimeter | GRE | [29] |
| | 1.5×10^{-9} | 1.2×10^{11} | 1978 | SIN | Calorimeter | GRE | [30,31] |
| Cu | 2.6×10^{-8} | 2.2×10^9 | 1972 | (CERN) | Spark chamber | GS/GRE | [32] |
| | 2.2×10^{-7} | | 1962 | | Spark chamber | | [33] |
| ^{127}I | 3×10^{-10} | 2.1×10^{12} | 1980 | | Radiochemical | GS | [25] |

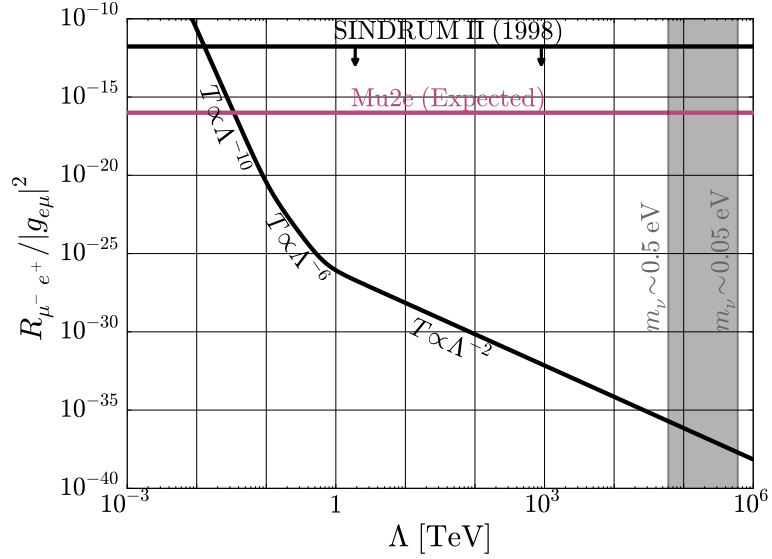


Figure 2. The estimation of the $\mu^- \rightarrow e^+$ rate, as a function of the new physics scale parameter Λ . Taken from [9]

2.2. Past $\mu^- \rightarrow e^+$ experiments

The results from past $\mu^- \rightarrow e^+$ experiments are listed in Table 1 [24]. The experimental techniques were similar for all of these searches, measuring the energy spectrum of positrons or counting the number of positrons in a signal window for the $\mu^- \rightarrow e^+$ signal from the muon beam interaction with a target, using a tracking detector, scintillator counter, or scintillating calorimeter. The experiment using ^{127}I as the nuclear target [25] used a radiochemical method: a NaI target material was irradiated with the muon beam, the target was chemically treated to extract ^{127}Sb or ^{127}Te , and the decay rate of ^{127}Te was measured.

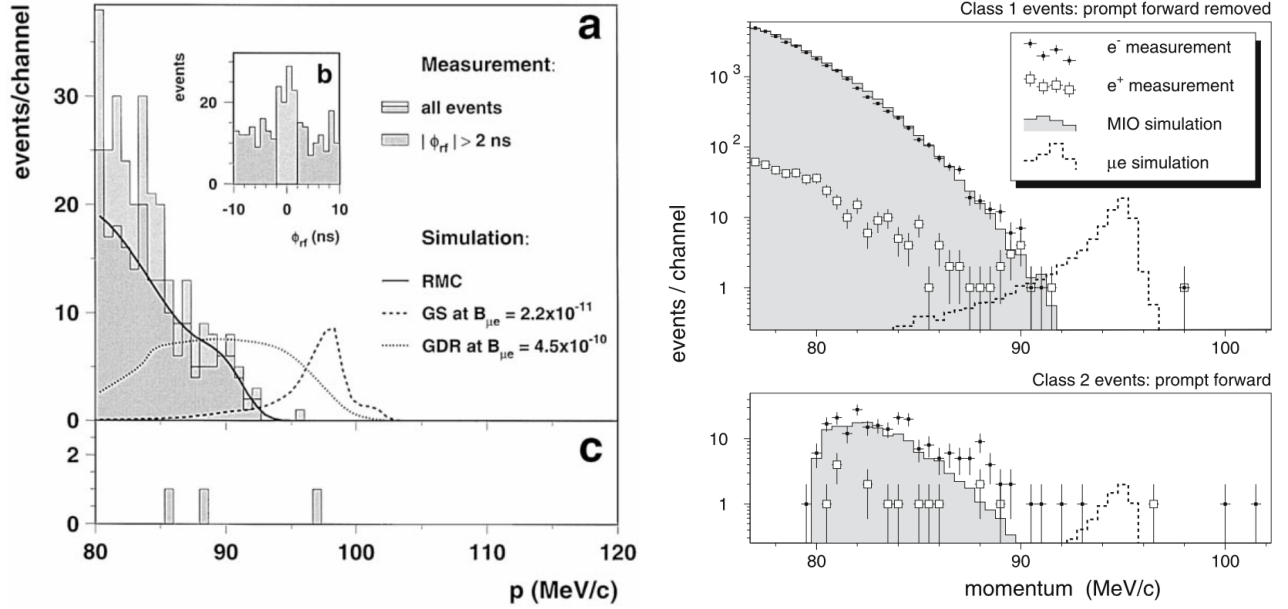


Figure 3. The energy spectrum of the signal estimation and backgrounds of $\mu^- \rightarrow e^+$ (left) and $\mu^- \rightarrow e^-$ (right) experiments. For $\mu^- \rightarrow e^+$, upper and lower plots are the data when the muon beam is on and off, respectively. For $\mu^- \rightarrow e^-$, upper and lower plots are the data with the possible RPC background removed, and RPC enhanced samples, respectively. They are shown for the signal shape comparison. These plots are from SINDRUM-II experiment result, and taken from Ref. [19] and [34].

Figure 3 shows the experimental result of the most recent $\mu^- \rightarrow e^+$ experiment [19] and compares it to the most recent result of the $\mu^- \rightarrow e^-$ experiment [34]. For $\mu^- \rightarrow e^+$, the nucleus in the final state can be either the ground state or an excited state. In the case of the transition to the ground state, the signal positron is mono-energetic with an energy ($E_{\mu^-e^+}$) given by:

$$E_{\mu^-e^+} = m_\mu + M(A, Z) - M(A, Z - 2) - B_\mu - E_{\text{recoil}}, \quad (6)$$

where m_μ is the muon mass, $M(A, Z)$ is the mass of the nucleus $N(A, Z)$, B_μ is the binding energy of the muonic atom, and E_{recoil} is the recoil energy of the outgoing nucleus. Similarly to photo-nuclear reactions, the $\mu^- \rightarrow e^+$ process may leave the target nuclei in a macroscopically excited state, a Giant Resonance, which is a collective multipole excitation of the protons in a nucleus against the neutrons [35]. For example, the Giant Dipole Resonance (GDR) with 20 MeV width was assumed in Ref. [19], resulting in a much wider energy distribution for the signal positron, as can be seen in Figure 3. Table A2 lists the $E_{\mu^-e^+}$ of the ground state transition for some selected nuclei popular in $\mu^- \rightarrow e^+$ experiments.

A potentially dominant physics background to $\mu^- \rightarrow e^+$ comes from radiative muon capture (RMC),

$$\mu^- + N(A, Z) \rightarrow \nu_\mu + N(A, Z - 1) + \gamma,$$

followed by photon pair production, $\gamma \rightarrow e^+ + e^-$, where the e^+ in the pair is misidentified as a signal. The photon energy spectrum of RMC, in particular in the endpoint energy region, is poorly known experimentally [36]. However, the maximum allowed endpoint energy ($E_{\text{RMC}}^{\text{end}}$) can be kinematically determined:

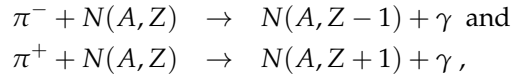
$$E_{\text{RMC}}^{\text{end}} = m_\mu + M(A, Z) - M(A, Z - 1) - B_\mu - E_{\text{recoil}}. \quad (7)$$

The endpoint energies of some popular nuclei are shown in Table A2. The nucleus in the final state may not be $N(A, Z - 1)$ once nucleon emission occurs. For this case, the RMC endpoint energy is smaller than that of Equation 7. It is also possible that the RMC endpoint energy could be much smaller depending on the spin state of the $N(A, Z)$ and $N(A, Z - 1)$ nuclei. In order to account for the RMC background, it is necessary to measure the RMC photon spectrum in a separate experiment. For example, the future COMET and Mu2e $\mu^- \rightarrow e^-$ experiments will be able to measure the RMC background before or along with the $\mu^- \rightarrow e^-$ data taking. Data from a dedicated experiment, such as the AlCap experiment [37], can also be useful. In addition, the kinematic separation of the RMC background and the $\mu^- \rightarrow e^+$ positron can be considered by choosing a proper target material such that the endpoint energy of RMC is smaller than the $\mu^- \rightarrow e^+$ positron energy, $E_{\text{RMC}}^{\text{end}} < E_{\mu^- e^+}$ [38], therefore:

$$M(A, Z - 2) < M(A, Z - 1). \quad (8)$$

RMC consideration in future experiments is described in detail in the next section.

Radiative pion capture (RPC),



followed by $\gamma \rightarrow e^+e^-$ is another background source, when the converted positron is misidentified as a signal. The RPC background can be controlled in $\mu^- \rightarrow e^+$ and $\mu^- \rightarrow e^-$ experiments by suppressing the pion contamination in the muon beam. A long beamline for sufficient pions to decay to muons could be considered. The pion/muon ratio of the beam was sufficiently small to achieve reasonable sensitivity in the previous $\mu^- \rightarrow e^-$ measurements, for example $\pi/\mu \sim 10^{-7}$ in the case of the SINDRUM II experiment [19]. It should be noted that the future COMET and Mu2e $\mu^- \rightarrow e^-$ experiments, which are targeting 100 - 10,000 times better sensitivities in $\mu^- \rightarrow e^-$ measurements, are adopting a pulsed proton beam with a high inter-beam particle extinction and a delayed data acquisition timing window technique in order to suppress the effect of pions (and particles other than muons) in the beam [4,5]. The future experimental setup of $\mu^- \rightarrow e^-$ and $\mu^- \rightarrow e^+$ experiments are described in detail in the next section.

Another serious background is cosmic-ray induced events. In general, the impact on backgrounds from cosmic-ray events is similar for $\mu^- \rightarrow e^-$ and $\mu^- \rightarrow e^+$ searches, therefore, consideration of detector design for suppressing the cosmic-ray backgrounds for $\mu^- \rightarrow e^-$ is applicable to the $\mu^- \rightarrow e^+$ case. For example, the future $\mu^- \rightarrow e^-$ experiments are adapting their cosmic-ray veto detector systems. In the case of a tracking detector design covering the muon stopping target, such as at COMET Phase-I, the cosmic-ray can be fully reconstructed, which will improve understanding of the effect from cosmic-rays [39]. Muon decay-in-orbit (DIO), which is one of the major background sources for $\mu^- \rightarrow e^-$, may also become background source in the $\mu^- \rightarrow e^+$ search if the photons generated from the interaction of the DIO electron near the endpoint energy with the detector material pair-creates a positron. It is not a serious background in the current target sensitivity level as long as the charge identification can be sufficiently achieved. However, it should be noted that the charge identification will never be perfect, especially in the case that an electron or positron is generated downstream of the detector system and propagates back to the muon stopping target.

3. Future $\mu^- \rightarrow e^+$ experimental searches

3.1. Upcoming experimental prospects

The COMET Phase-I [4] and Mu2e [5] experiments will have unprecedented sensitivity to $\mu^- \rightarrow e^+$ using aluminum as their nuclear targets, with single event sensitivities (SES) on the order of 10^{-15} and 10^{-17} respectively in the $\mu^- \rightarrow e^-$ conversion search. These experiments are expected to have similar sensitivities in the $\mu^- \rightarrow e^+$ channel. After COMET Phase-I, the detector will be upgraded for COMET Phase-II which will have an SES on the order of $\sim 10^{-17} - 10^{-18}$ [4]. There has also been an expression of interest in upgrading the Mu2e detector, called Mu2e-II, with an SES on the order of 10^{-18} [40].

Both experiments use similar principles to search for the $\mu^- \rightarrow e^-$ and $\mu^- \rightarrow e^+$ processes: (1) a pulsed proton beam is used to generate pions and muons in a production target within a superconducting solenoid; (2) the low momentum pions and muons are guided by the superconducting production solenoid field to a curved transport superconducting solenoid, which has an acceptance designed to eliminate high momentum particles; (3) an off-axis collimator selects the desired charge of the beam, utilizing the sign-dependent drift of the beam along the curved beamline; (4) the muons from production and pion decays along the beamline are stopped in a nuclear target within a superconducting solenoid containing the cylindrical detector elements; (5) non-stopped beam particles continue through the solenoid, passing through a central axis hole in the detector elements; (6) after a time sufficient for nearly all pions to either decay or be captured on the nuclear target, signal candidates are reconstructed in the detectors (where the central holes blind them to the high intensity, low momentum muon decay backgrounds). The pulsed proton beam significantly reduces beam related backgrounds during the signal measurement period, but this time delay method requires that the lifetime of the muon in the nuclear target (see Table A2) is large enough that there are a sufficient number of muon captures/decays in the target during the signal search period. Due to this restriction, nuclear target materials with $Z \gtrsim 40$ cannot be easily studied at experiments like COMET and Mu2e.

3.2. RMC status

Both COMET and Mu2e will also have far greater sensitivity to the high momentum positron spectrum from RMC than previous muon conversion and RMC measurement experiments. The background arises from highly asymmetric RMC photon conversions, either from real (on-shell) photons converting in the detector material or virtual (off-shell) photons internally converting, and the background significantly depends on the nuclear target. The internal conversion spectrum for RMC has never been measured, though the internal conversion spectrum approximation from Kroll and Wada [41] (with corrections published by Joseph [42]) for general nuclear captures with RPC in mind should similarly apply for RMC, as shown by Plestid and Hill [43]. This approximation makes simplifying assumptions about the e^+e^- matrix element by using the energy spectrum of the on-shell photon and assumes that the virtuality of the e^+e^- pair is small. Following this, the internal conversion spectrum can be estimated directly from the on-shell photon spectrum, requiring only an on-shell photon spectrum to predict the total on- and off-shell photon spectrum. Plestid and Hill show that this approximation is most reliable in the high energy region of the electron/positron spectra, with the next order uncertainty decreasing as the positron energy approaches the endpoint [43].

The on-shell RMC photon spectrum was measured by the TRIUMF RMC Spectrometer group on several nuclear targets, including aluminum [36,44–46]. As the experiment was interested in studying g_p/g_n , these measurements were focused on the total rate of RMC, not accurately modeling or measuring the high energy tail. The closure approximation is typically used to describe the RMC photon energy spectrum, where one assumes the sum of the nuclear final states can be approximated with a single nuclear transition using the mean excitation

energy. This nuclear excitation energy manifests as the closure approximation endpoint, and is typically considered a free parameter that is fit to data. The closure approximation photon energy spectrum is shown in Equation 9, where $x = E_\gamma/k_{\max}$ and k_{\max} is the spectrum endpoint [47,48]:

$$\frac{dn}{dx} = \frac{e^2 k_{\max}^2}{\pi m_\mu^2} \left(1 - \frac{N-Z}{A}\right) (1 - 2x + 2x^2)x(1-x)^2. \quad (9)$$

The TRIUMF RMC Spectrometer group measured a closure approximation endpoint of 90.1 ± 1.8 MeV and a branching fraction of $(1.40 \pm 0.11) \times 10^{-5}$ above 57 MeV with respect to ordinary muon capture (OMC) using aluminum as their nuclear target [36]. This endpoint is significantly lower than the kinematic endpoint on aluminum, ~ 101.9 MeV, as shown in Appendix A. This was the case for all of the nuclear targets - the fit closure approximation endpoint was ~ 10 MeV below the target's kinematic endpoint. As nothing forbids photon energies up to the kinematic endpoint, there is no reason to expect the spectrum to be 0 between the measured endpoint and the kinematic endpoint, though it may be suppressed. Predictions using a Fermi gas model by Fearing et al. [49,50] show the photon energy spectrum falling up to the kinematic endpoint, with no tuned endpoint as found in the closure approximation. A few example spectra from these calculations are shown in Figure 4.

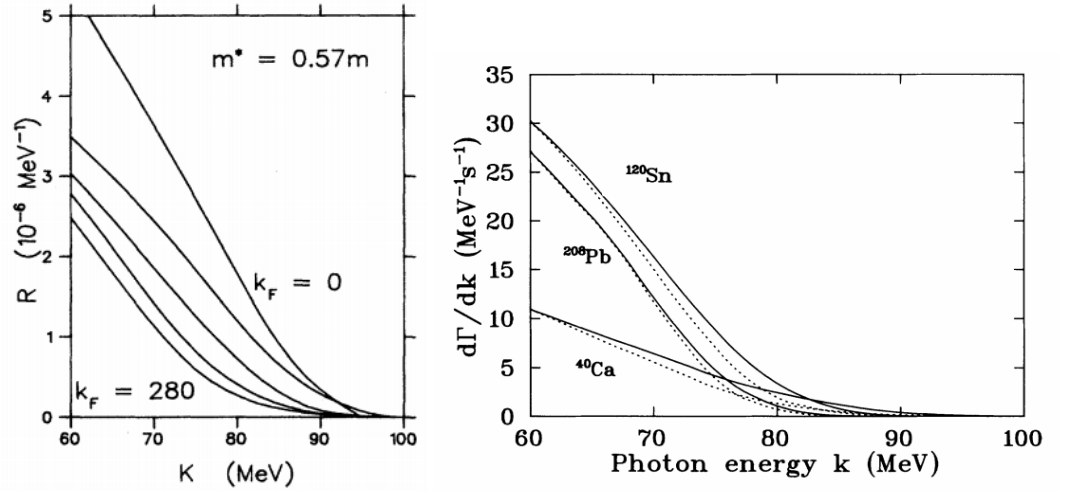


Figure 4. RMC spectra vs k_{Fermi} [49] (left) and example RMC spectra [50] (right) as calculated using a Fermi gas model.

On aluminum, the nuclear target for the currently planned COMET Phase-I and Mu2e searches, the ground state transition energy for the positron signal is 92.3 MeV, far below the RMC kinematic endpoint of ~ 101.9 MeV. Unlike the $\mu^- \rightarrow e^-$ searches, DIO backgrounds are not a significant background in the positron channel at the sensitivity level of the current and future experiments, so the dominant backgrounds are RMC, RPC, antiprotons, and cosmic-ray events. The non-RMC backgrounds are expected to contribute similarly in the positron and electron channel, where the expectation is less than 1 event per experiment for both searches [4,5], but RMC is the greatest unknown in this channel. Assuming the closure approximation with the measured endpoint, the true positron spectrum would end at 89.6 ± 1.8 MeV/c with a rapidly falling spectrum, so only resolution and energy loss effects would lead to overlaps with the signals. As the resolution is $\mathcal{O}(200 \text{ keV}/c)$ for both experiments [4,5] and the two processes are separated by nearly 3 MeV/c, both experiments

would be able to maintain a background expectation of below 1 event per experiment for the measured endpoint.

The dataset on aluminum for the 1999 RMC measurement from TRIUMF only had $\mathcal{O}(3,000)$ photons above 57 MeV (the region in which TRIUMF's measurement was performed), so they were not sensitive to photon rates above 90 MeV that are about 3,000 times smaller than the total rate above 57 MeV ($R(E_\gamma > 90 \text{ MeV}) = \frac{\Gamma_{RMC}(E_\gamma > 57 \text{ MeV})}{\Gamma_{OMC}}$). COMET Phase-I and Mu2e will see about 10^{16} and 10^{18} muon captures respectively [4,5], and so will have $\sim 10^{11}$ and 10^{13} RMC photons above 57 MeV. To test their sensitivity to RMC beyond the fit endpoint on aluminum, we can assume a flat photon energy spectrum tail above 90 MeV up to the kinematic endpoint with a rate around the limit TRIUMF's sensitivity, shown in Equation 10.

$$R(E_\gamma > 90 \text{ MeV}) = \frac{1}{3,000} \times R(E_\gamma > 57 \text{ MeV}) = 4.7 \times 10^{-9} \quad (10)$$

We also make the following simplifying assumptions: the photon conversion energy sharing spectrum is flat, there is a 0.1% chance of a photon conversion in the nuclear target, and the tracking efficiency for $\sim 90 \text{ MeV}/c$ positrons is 10%. This leads to a positron background rate of $\mathcal{O}(500)$ and $\mathcal{O}(50,000)$ events per MeV/c at 90 MeV/c for COMET Phase-I and Mu2e respectively, before even considering internal photon conversions, as shown in Figure 5. In this simple model, which is consistent with the existing data on aluminum, the RMC background would significantly alter the search strategy (e.g. performing a momentum spectrum fit and loosening the cuts suppressing other backgrounds instead of a cut-and-count search with tight suppression of other backgrounds) and impact the discovery potential of $\mu^- \rightarrow e^+$ signal searches.

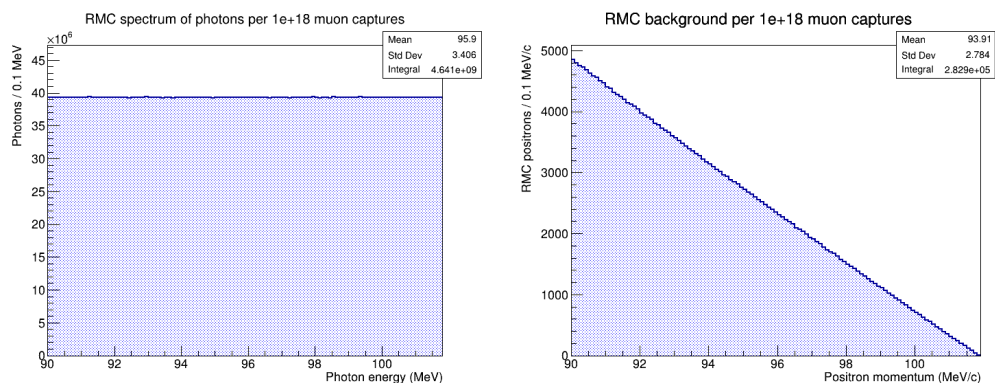


Figure 5. Assumed on-shell photon RMC spectrum high energy tail on aluminum for 10^{18} muon captures (left) and the corresponding positron spectrum using the simplifying assumptions about the conversion spectrum and track reconstruction (right).

3.3. RMC considerations at future LFV experiments

The discovery potential of future experiments searching for $\mu^- \rightarrow e^+$ is entwined with their understanding of the RMC background, where any claim of new physics must also be able to accurately subtract the SM background. As the RMC spectrum is not well constrained by existing measurements, muon conversion experiments should plan to perform RMC measurements on the relevant nuclear targets. COMET is planning to measure the on-shell photon spectrum using photon conversion in the inner wall of the cylindrical tracker, reconstructing the e^+e^- pair constrained to a vertex consistent with this wall [4]. At Mu2e, a photon measurement could be done by using a lower beam intensity and a thin photon converter added to the

detector to increase the conversion efficiency. The magnetic field at Mu2e could be lowered to increase the tracking efficiency for low momentum tracks, where the requirement of two opposite signed tracks consistent with either the photon converter (on-shell photons) or the nuclear target (on- and off-shell photons) is used to reduce backgrounds. Mu2e could also use the calorimeter to measure the on-shell photon spectrum directly, where a lower beam intensity may be necessary to reduce pileup backgrounds. A higher radial cluster requirement, a rejection of clusters matched to reconstructed tracks, and a requirement that the shower shape is more consistent with a photon than an electron can reduce beam and DIO backgrounds. The direct measurement of the on-shell photon spectrum at either experiment would also allow for a measurement of the positron spectrum from off-shell photons by subtracting the expected contribution from the measured on-shell spectrum, a direct test of the predictions by Plestid and Hill [43].

Future muon conversion experiments can also consider choosing a nuclear target whose $\mu^- \rightarrow e^+$ ground state transition energy is above the kinematic endpoint of the RMC spectrum, kinematically suppressing this background. This translates into a requirement that the nuclear mass of $N(A, Z-2)$ is smaller than the nuclear mass of $N(A, Z-1)$. Several potential target choices were identified by Yeo et al. [38], where all of the nuclear targets considered had $\mu^- \rightarrow e^+$ ground state transition energies greater than the RMC kinematic endpoints. For each nuclear target considered, the authors assumed a closure approximation with the endpoint set to be the kinematic endpoint and the branching fraction above 57 MeV to be the measured value by the TRIUMF RMC Spectrometer group. For an example 10^{18} muon stops, they found COMET Phase-II would be able to achieve limits with 90% C.L. of $\mathcal{O}(10^{-15})$ for the ground state transition, three orders of magnitude improved upon the current limit from Ref. [19]. This is compared to the perhaps not even one order of magnitude potential gain by using aluminum as the nuclear target [38], showing how critical the nuclear target choice can be for the $\mu^- \rightarrow e^+$ search.

These potential upper limits importantly do not include an assessment of the impact on the limit due to the systematic uncertainty on the RMC background modeling. The closure approximation does not take into account exclusive transitions to low lying states, which could lead to a more complicated background spectrum with kinks or knees in the photon energy spectrum. These are likely to be smoothed by the (internal) pair conversion spectrum, but without understanding the RMC spectrum it will be difficult to have confidence in a low statistics discovery claim $\mu \rightarrow e$ experiments are typically capable of ($\mathcal{O}(5 - 10)$ events). As the goal of these searches is to discover new physics, the experiments must be prepared for the potential discovery of the LNV $\mu^- \rightarrow e^+$ process, which requires the confident rejection of RMC as an alternate hypothesis.

4. Concluding remarks: Towards future $\mu^- \rightarrow e^+$ measurements

CLFV is a long sought-after signal of physics beyond the SM. Many experiments have searched for $\mu^- \rightarrow e^-$ and $\mu^- \rightarrow e^+$ processes, where the result is strongly complementary to the most stringent CLFV channel, $\mu \rightarrow e\gamma$. The $\mu^- \rightarrow e^+$ process is also an LNV channel, which may give insight into the Majorana property of the neutrino. Although it is not as strong a channel as $0\nu\beta\beta$ is in general, its discovery would provide insight on the flavor effects in the neutrino mass generation. Current and future experiments will have unprecedented sensitivity to both $\mu^- \rightarrow e^-$ and $\mu^- \rightarrow e^+$ processes. However, the search for $\mu^- \rightarrow e^+$ requires more careful considerations in terms of nuclear target selection in order to reach the full discovery potential of these experiments.

RMC is one of the least understood backgrounds at $\mu \rightarrow e$ experiments, with potential to be the largest background in the $\mu^- \rightarrow e^+$ search. RMC is theoretically understudied, and previous RMC measurements do not have the necessary sensitivity in the high energy photon

region to sufficiently constrain this background at the currently planned COMET Phase-I and Mu2e experiments. These experiments will need to measure the RMC photon energy spectrum, as well as the internal conversion spectrum, in order to confidently reject the SM backgrounds in the case of a $\mu^- \rightarrow e^+$ signal.

An important consideration for the currently planned COMET and Mu2e experiments using aluminum as their nuclear target is what the next steps will be if they discover the process of $\mu^- \rightarrow e^+$. In the $\mu^- \rightarrow e^-$ search, the typical idea is to try to determine the nature of the beyond the SM physics by testing the nuclear target dependence of the conversion rate. A calculation of the $\mu^- \rightarrow e^-$ rate dependence on the nuclear target for a few example new physics models is shown in Figure 6. For nuclear targets with Z below 40, most of the models vary by $\sim 10\text{-}20\%$, where only the penguin model varies significantly from the other models at higher Z . Mu2e, for example, will have an uncertainty of $\sim 10\%$ on the total number of muon captures for a given target, likely uncorrelated between targets, and so will have an uncertainty of at least $\sim 15\%$ when comparing the rates between models for even a high statistics measurement. The statistical precision necessary for such a comparison would require a measurement of more than 100 signal events, far beyond the threshold of $\sim 5\text{-}10$ events needed to claim a discovery in the $\mu^- \rightarrow e^-$ channel [5].

In the $\mu^- \rightarrow e^+$ case, there is more than the ground state transition to consider. Experiments can search for the GDR transition in addition to the ground-state transition, and measure the relative rate between the ground state and the GDR transition. As this is a ratio, and therefore independent of the number of muon captures, it is possible this can be better used to test the dependence on the nuclear target, helping to understand the underlying mechanism for the LNV process. The nuclear dependence of the $\mu^- \rightarrow e^+$ process needs to be further studied to determine the potential next steps experiments should take in the case of $\mu^- \rightarrow e^+$ discovery.

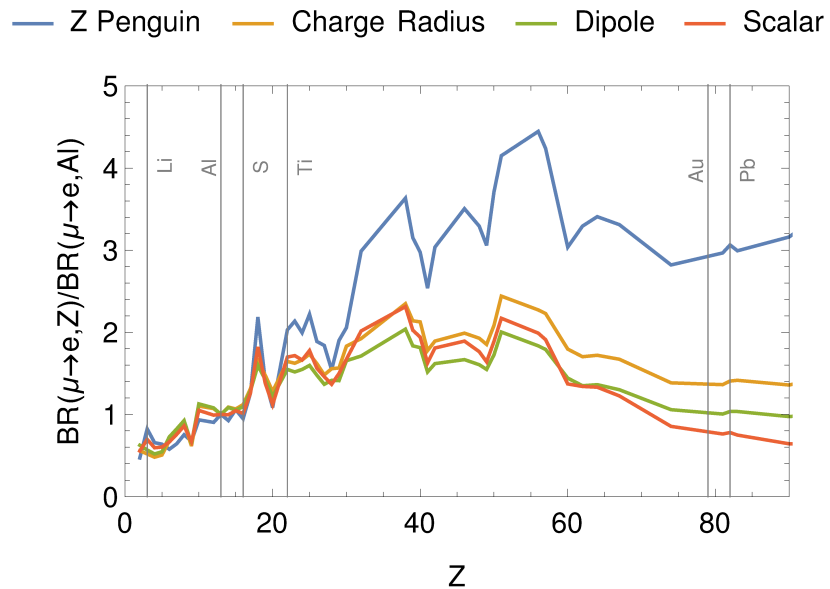


Figure 6. Relative rate of $\mu^- \rightarrow e^-$ with respect to the rate on aluminum for several example models taken from Ref. [51] and based on the calculations by Ref. [52] and [53].

Appendix A RMC endpoint calculation on aluminum

The RMC kinematic endpoint on aluminum can be calculated by considering the “decay” of the $\mu^- N(A, Z)$ system to $\gamma N(A, Z - 1)v_\mu$ with $p(v_\mu) = 0$, which is then a two body decay

with a photon energy given by Equation 7. Since the muon is ~ 200 times heavier than the electron, and therefore has a much closer orbit in the atom, the electrons do not participate in the process. The relevant masses are then the muon mass and the incoming and outgoing nuclei, not the atomic masses, where the nuclear mass is given by $M(A, Z) = M_A - Z \cdot m_e$, where $M_A = A_r \cdot u$, A_r is the relative mass, u is the atomic mass unit, and m_e is the electron mass. The final state particles then satisfy $p_\gamma = -p_{27Al}$ and the energy of the recoiling magnesium nucleus is given by:

$$E_{27Mg} = \frac{M^2 + M_N(^{27}Mg)^2}{2M} = E_{\text{recoil}} + M_N(^{27}Mg) \quad (\text{A1})$$

where M is the mass of the muonic aluminum system, $M = M(^{27}Al) + m_\mu - B_\mu$. Table A1 shows the input parameters for Equations A1 and 7, where the resulting kinematic RMC endpoint on aluminum is 101.867 MeV. The corresponding positron energy that will be measured by $\mu^- \rightarrow e^+$ experiments is one positron mass below this, which is listed in Table A2 for some example nuclei.

Table A1. Parameters used in the RMC endpoint energy calculation on aluminum.

| Parameter | Value |
|---------------------|--------------------------------------|
| m_μ | 105.6583745 MeV/c ² [54] |
| m_e | 0.5109989461 MeV/c ² [54] |
| $1u$ | 931.49410242 MeV/c ² [54] |
| B_μ | 0.464 MeV [55] |
| $A_r(^{27}Al)$ | 26.98153841 u [56] |
| $M_N(^{27}Al)$ | 25126.501 MeV/c ² |
| $A_r(^{27}Mg)$ | 26.98434063 u [56] |
| $M_N(^{27}Mg)$ | 25129.622 MeV/c ² |
| E_{recoil} | 0.206 MeV/c ² |

Table A2. The energy of the signal positron ($E_{\mu^-e^+}$) obtained from Equation 6, the RMC positron endpoint energy ($E_{\text{RMC}}^{\text{end}}$) of the ground state transition obtained from Equation 7, and the lifetime of the muonic atom (τ_{μ^-}) of some nuclei popular in $\mu^- \rightarrow e^+$ experiments. The energy of the signal electron ($E_{\mu^-e^-}$) for $\mu^- \rightarrow e^-$ are also shown for comparison. Nuclear masses required for these calculations are taken from AME2016 data [56]. The lifetime data is from Ref. [57].

| Nuclide | $E_{\mu^-e^+}$ [MeV] | $E_{\text{RMC}}^{\text{end}}$ [MeV] | τ_{μ^-} [ns] | $E_{\mu^-e^-}$ [MeV] |
|------------------|----------------------|-------------------------------------|---------------------|----------------------|
| ²⁷ Al | 92.30 | 101.36 | 864 | 104.97 |
| ³² S | 101.80 | 102.03 | 555 | 104.76 |
| ⁴⁸ Ti | 98.89 | 104.18 | 329 | 104.18 |

Author Contributions: Writing—original draft preparation, M. L. and M. M.; writing—review and editing, M.L. and M. M. All authors have read and agreed to the published version of the manuscript.

Funding: This research of M.L. was supported by Institute for Basic Science (IBS-R017-D1-2021-a00) of Korea. This research of M.M. was in part funded by the “Research in the Energy, Cosmic and Intensity Frontiers at Northwestern University” award, DE-SC0015910.

Institutional Review Board Statement: Not applicable.

Informed Consent Statement: Not applicable.

Data Availability Statement: The data used in this study can be provided by the authors upon request.

Acknowledgments: The authors M.L. and M.M. are collaborators of the COMET and Mu2e collaborations, respectively. The author M.L. thanks KEK and J-PARC, Japan for their support of infrastructure and the operation of COMET. This work of M.L. is supported in part by: Japan Society for the Promotion of Science (JSPS) KAKENHI Grant Nos. 25000004 and 18H05231; JSPS KAKENHI Grant No.JP17H06135; Belarusian Republican Foundation for Fundamental Research Grant F18R-006; National Natural Science Foundation of China (NSFC) under Contracts No. 11335009 and 11475208; Research program of the Institute of High Energy Physics (IHEP) under Contract No. Y3545111U2; the State Key Laboratory of Particle Detection and Electronics of IHEP, China, under Contract No.H929420BTD; Supercomputer funding in Sun Yat-Sen University, China; National Institute of Nuclear Physics and Particle Physics (IN2P3), France; Shota Rustaveli National Science Foundation of Georgia (SRNSFG), grant No. DI-18-293; Deutsche Forschungsgemeinschaft grant STO 876/7-1 of Germany; Joint Institute for Nuclear Research (JINR), project COMET #1134; Institute for Basic Science (IBS) of Republic of Korea under Project No. IBS-R017-D1-2021-a00; Ministry of Education and Science of the Russian Federation and by the Russian Fund for Basic Research grants: 17-02-01073, 18-52-00004; Science and Technology Facilities Council, United Kingdom; JSPS London Short Term Predoctoral Fellowship program, Daiwa Anglo-Japanese Foundation Small Grant; and Royal Society International Joint Projects Grant. The author M.M. is grateful for the vital contributions of the Fermilab staff and the technical staff of the participating institutions to Mu2e. This work was supported by the US Department of Energy; the Istituto Nazionale di Fisica Nucleare, Italy; the Science and Technology Facilities Council, UK; the Ministry of Education and Science, Russian Federation; the National Science Foundation, USA; the Thousand Talents Plan, China; the Helmholtz Association, Germany; and the EU Horizon 2020 Research and Innovation Program under the Marie Skłodowska-Curie Grant Agreement No. 690835, 734303, 822185, 858199. This document was prepared in part by members of the Mu2e Collaboration using the resources of the Fermi National Accelerator Laboratory (Fermilab), a U.S. Department of Energy, Office of Science, HEP User Facility. Fermilab is managed by Fermi Research Alliance, LLC (FRA), acting under Contract No. DE-AC02-07CH11359.

Conflicts of Interest: The authors declare no conflict of interest.

References

- Baldini, A. M.; et al. (MEG collaboration). Search for the lepton flavour violating decay $\mu^+ \rightarrow e^+ \gamma$ with the full dataset of the MEG experiment. *The European Physical Journal C* **2016**, *76*, 434. doi:10.1140/epjc/s10052-016-4271-x.
- Baldini, A. M.; et al. (MEG collaboration). The Search for $\mu^+ \rightarrow e^+ \gamma$ with 10^{-14} Sensitivity: The Upgrade of the MEG Experiment. *Symmetry* **2021**, *13*. doi:10.3390/sym13091591.
- Arndt K.; et al. (Mu3e collaboration). Technical design of the phase I Mu3e experiment. *Nuclear Instruments and Methods in Physics Research Section A: Accelerators, Spectrometers, Detectors and Associated Equipment* **2021**, *1014*, 165679. doi:https://doi.org/10.1016/j.nima.2021.165679
- Abramishvili, R.; et al. (COMET collaboration). COMET Phase-I technical design report. *Progress of Theoretical and Experimental Physics* **2020**, *2020*, [https://academic.oup.com/ptep/article-pdf/2020/3/033C01/32903980/ptz125.pdf]. 033C01, doi:10.1093/ptep/ptz125.
- Bartoszek, L.; et al. (Mu2e collaboration). Mu2e Technical Design Report, 2015, [arXiv:physics.ins-det/1501.05241].
- Marciano, W.J.; Mori, T.; Roney, J.M. Charged Lepton Flavor Violation Experiments. *Annual review of nuclear and particle science* **2008**, *58*, 315–341.
- Amhis, Y.; et al. (Heavy Flavor Averaging Group (HFLAV)). Averages of b-hadron, c-hadron, and τ -lepton properties as of 2018. *European Physical Journal C* **2021**, *81*, 226. doi:10.1140/epjc/s10052-020-8156-7.
- Gando, Y. First results of KamLAND-Zen 800. *Journal of Physics: Conference Series* **2020**, *1468*, 012142. doi:10.1088/1742-6596/1468/1/012142.
- Berryman, J.M.; de Gouvêa, A.; Kelly, K.J.; Kobach, A. Lepton-number-violating searches for muon to positron conversion. *Phys. Rev. D* **2017**, *95*, 115010. doi:10.1103/PhysRevD.95.115010.
- Geib, T.; Merle, A.; Zuber, K. $\mu^- - e^+$ conversion in upcoming LFV experiments. *Physics Letters B* **2017**, *764*, 157 – 162. doi:https://doi.org/10.1016/j.physletb.2016.11.029.
- Geib, T.; Merle, A. $\mu^- - e^+$ conversion from short-range operators. *Phys. Rev. D* **2017**, *95*, 055009. doi:10.1103/PhysRevD.95.055009.
- Chen, C.S.; Geng, C.Q.; Ng, J.N. Unconventional neutrino mass generation, neutrinoless double beta decays, and collider phenomenology. *Phys. Rev. D* **2007**, *75*, 053004. doi:10.1103/PhysRevD.75.053004.
- King, S.F.; Merle, A.; Panizzi, L. Effective theory of a doubly charged singlet scalar: complementarity of neutrino physics and the LHC. *JHEP* **2014**, *2014*, 124. doi:10.1007/JHEP11(2014)124.

14. Pritimita, P.; Dash, N.; Patra, S. Neutrinoless Double Beta Decay in LRSM with Natural Type-II seesaw Dominance. *JHEP* **2016**, *2016*, 147, [[arXiv:hep-ph/1607.07655](https://arxiv.org/abs/1607.07655)]. doi:10.1007/JHEP10(2016)147.
15. Cirigliano, V.; Kurylov, A.; Ramsey-Musolf, M.J.; Vogel, P. Neutrinoless Double Beta Decay and Lepton Flavor Violation. *Phys. Rev. Lett.* **2004**, *93*, 231802. doi:10.1103/PhysRevLett.93.231802.
16. Engel, J.; Menéndez, J. Status and future of nuclear matrix elements for neutrinoless double-beta decay: a review. *Reports on Progress in Physics* **2017**, *80*, 046301. doi:10.1088/1361-6633/aa5bc5.
17. Miyazaki, Y.; et al. (Belle collaboration). Search for lepton-flavor and lepton-number-violating $\tau \rightarrow \ell h h'$ decay modes. *Physics Letters B* **2013**, *719*, 346–353. doi:<https://doi.org/10.1016/j.physletb.2013.01.032>.
18. Cortina Gil, E.; et al. (NA62 collaboration). Searches for lepton number violating K^+ decays. *Physics Letters B* **2019**, *797*, 134794. doi:<https://doi.org/10.1016/j.physletb.2019.07.041>.
19. Kaulard, J.; Dohmen, C.; Haan, H.; Honecker, W.; Junker, D.; Otter, G.; Starlinger, M.; Wintz, P.; Hofmann, J.; Bertl, W.; Egger, J.; Krause, B.; Egli, S.; Engfer, R.; Findeisen, C.; Hermes, E.; Kozlowski, T.; Niebuhr, C.; Rutsche, M.; Pruys, H.; van der Schaaf, A. Improved limit on the branching ratio of $\mu^- \rightarrow e^+$ conversion on titanium. *Physics Letters B* **1998**, *422*, 334–338. doi:[https://doi.org/10.1016/S0370-2693\(97\)01423-8](https://doi.org/10.1016/S0370-2693(97)01423-8).
20. Domin, P.; Kovalenko, S.; Faessler, A.; Šimkovic, F. Nuclear (μ^-, e^+) conversion mediated by Majorana neutrinos. *Phys. Rev. C* **2004**, *70*, 065501. doi:10.1103/PhysRevC.70.065501.
21. Atre, A.; Barger, V.; Han, T. Upper bounds on lepton-number violating processes. *Phys. Rev. D* **2005**, *71*, 113014. doi:10.1103/PhysRevD.71.113014.
22. Ejiri, H. Nuclear Matrix Elements for β and $\beta\beta$ Decays and Quenching of the Weak Coupling g_A in QRPA. *Frontiers in Physics* **2019**, *7*, 30. doi:10.3389/fphy.2019.00030.
23. Vergados, J.D.; Ejiri, H.; Šimkovic, F. Theory of neutrinoless double-beta decay. *Reports on Progress in Physics* **2012**, *75*, 106301. doi:10.1088/0034-4885/75/10/106301.
24. Particle Data Group. Review of Particle Physics. *Progress of Theoretical and Experimental Physics* **2020**, *2020*, [<https://academic.oup.com/ptep/article/2020/8/083C01/34673722/ptaa104.pdf>]. 083C01, doi:10.1093/ptep/ptaa104.
25. Abela, R.; Backenstoss, G.; Kowald, W.; Wüest, J.; Seiler, H.; Seiler, M.; Simons, L. New upper limit for $\mu^- \rightarrow e^+$ conversion. *Physics Letters B* **1980**, *95*, 318–322. doi:[https://doi.org/10.1016/0370-2693\(80\)90495-5](https://doi.org/10.1016/0370-2693(80)90495-5).
26. Kaulard, J.Q. Suche nach der Verbotenen Ladungsaustauschenden Mye-konversion $\mu^- \text{ Ti} \rightarrow e^+ \text{ Ca}$ (Search for forbidden charge exchanging μe conversion $\mu^- \text{ Ti} \rightarrow e^+ \text{ Ca}$). PhD thesis, RWTH Aachen university, 1997.
27. Dohmen, C.; Groth, K.D.; Heer, B.; Honecker, W.; Otter, G.; Steinrücken, B.; Wintz, P.; Djordjadze, V.; Hofmann, J.; Kozlowski, T.; Playfer, S.; Bertl, W.; Egger, J.; Herold, W.; Krause, B.; Walter, H.; Engfer, R.; Findeisen, C.; Grossmann-Handschin, M.; Hermes, E.; Muheim, F.; Niebuhr, C.; Pruys, H.; Ricken, L.; Vermeulen, D.; van der Schaaf, A. Test of lepton-flavour conservation in $\mu \rightarrow e$ conversion on titanium. *Physics Letters B* **1993**, *317*, 631–636. doi:[https://doi.org/10.1016/0370-2693\(93\)91383-X](https://doi.org/10.1016/0370-2693(93)91383-X).
28. Ahmad, S.; Azuelos, G.; Blecher, M.; Bryman, D.A.; Burnham, R.A.; Clifford, E.T.H.; Depommier, P.; Dixit, M.S.; Gotow, K.; Hargrove, C.K.; Hasinoff, M.; Leitch, M.; Macdonald, J.A.; Mes, H.; Navon, I.; Numao, T.; Poutissou, J.M.; Poutissou, R.; Schlatter, P.; Spuller, J.; Summhammer, J. Search for muon-electron and muon-positron conversion. *Phys. Rev. D* **1988**, *38*, 2102–2120. doi:10.1103/PhysRevD.38.2102.
29. Badertscher, A.; et al. New Upper Limits for Muon - Electron Conversion in Sulfur. *Lett. Nuovo Cim.* **1980**, *28*, 401–408. doi:10.1007/BF02776193.
30. Badertscher, A.; Borer, K.; Czapek, G.; Flückiger, A.; Hänni, H.; Hahn, B.; Hugentobler, E.; Kaspar, H.; Markees, A.; Moser, U.; Redwine, R.; Schacher, J.; Scheidiger, H.; Schlatter, P.; Viertel, G. Search for $\mu^- \rightarrow e^+$ conversion on sulfur: A. Badertscher et. al., *Phys. Lett.* **79B** (1978) 371. *Physics Letters B* **1979**, *80*, 434. doi:[https://doi.org/10.1016/0370-2693\(79\)91214-0](https://doi.org/10.1016/0370-2693(79)91214-0).
31. Badertscher, A.; Borer, K.; Czapek, G.; Flückiger, A.; Hänni, H.; Hahn, B.; Hugentobler, E.; Kaspar, H.; Markees, A.; Moser, U.; Redwine, R.; Schacher, J.; Scheidiger, H.; Schlatter, P.; Viertel, G. Search for $\mu^- \rightarrow e^+$ conversion on sulfur. *Physics Letters B* **1978**, *79*, 371–375. doi:[https://doi.org/10.1016/0370-2693\(78\)90385-4](https://doi.org/10.1016/0370-2693(78)90385-4).
32. Bryman, D.A.; Blecher, M.; Gotow, K.; Powers, R.J. Search for the Reaction $\mu^- + \text{Cu} \rightarrow e^+ + \text{Co}$. *Phys. Rev. Lett.* **1972**, *28*, 1469–1471. doi:10.1103/PhysRevLett.28.1469.
33. Conforto, G.; Conversi, M.; Lella, L.d.; Penso, G.; Rubbia, C.; Toller, M. Search for Neutrinoless Coherent Nuclear Capture of μ^- Mesons. *Il Nuovo Cimento* **1962**, *26*, 261–281. doi:<https://doi.org/10.1007/BF02787041>.
34. Bertl, W.; Engfer, R.; Hermes, E.A.; Kurz, G.; Kozlowski, T.; Kuth, J.; Otter, G.; Rosenbaum, F.; Ryskulov, N.M.; van der Schaaf, A.; Wintz, P.; Zychor, I.; Collaboration, T.S.I. A search for μ -e conversion in muonic gold. *The European Physical Journal C - Particles and Fields* **2006**, *47*, 337–346. doi:10.1140/epjc/s2006-02582-x.
35. Snover, K.A. Giant Resonances in Excited Nuclei. *Annual Review of Nuclear and Particle Science* **1986**, *36*, 545–603, [<https://doi.org/10.1146/annurev.ns.36.120186.002553>]. doi:10.1146/annurev.ns.36.120186.002553.

36. Bergbusch, P.C.; Armstrong, D.S.; Blecher, M.; Chen, C.Q.; Doyle, B.C.; Gorringer, T.P.; Gumplinger, P.; Hasinoff, M.D.; Jonkmans, G.; Macdonald, J.A.; Poutissou, J.M.; Poutissou, R.; Sigler, C.N.; Wright, D.H. Radiative muon capture on O, Al, Si, Ti, Zr, and Ag. *Phys. Rev. C* **1999**, *59*, 2853–2864. doi:10.1103/PhysRevC.59.2853.
37. Edmonds, A. Latest Updates from the AlCap Experiment. 13th Conference on the Intersections of Particle and Nuclear Physics, 2018, [[arXiv:physics.ins-det/1809.10122](https://arxiv.org/abs/physics.ins-det/1809.10122)].
38. Yeo, B.; Kuno, Y.; Lee, M.; Zuber, K. Future experimental improvement for the search of lepton-number-violating processes in the $e\mu$ sector. *Phys. Rev. D* **2017**, *96*, 075027. doi:10.1103/PhysRevD.96.075027.
39. Wong, T.S. Study of Negative Muon to Positron Conversion in the COMET Phase-I experiment. PhD thesis, Osaka university, 2020.
40. Abusalma, F.; et al.. Expression of Interest for Evolution of the Mu2e Experiment, 2018, [[arXiv:physics.ins-det/1802.02599](https://arxiv.org/abs/physics.ins-det/1802.02599)].
41. Kroll, N.M.; Wada, W. Internal Pair Production Associated with the Emission of High-Energy Gamma Rays. *Phys. Rev.* **1955**, *98*, 1355–1359. doi:10.1103/PhysRev.98.1355.
42. Joseph, D.W. Electron pair creation in π^+p capture reactions from rest. *Il Nuovo Cimento* **1960**, *16*, 997–1013. doi:10.1007/BF02860383.
43. Plestid, R.; Hill, R.J. The high energy spectrum of internal positrons from radiative muon capture on nuclei, 2020, [[arXiv:hep-ph/2010.09509](https://arxiv.org/abs/hep-ph/2010.09509)].
44. Armstrong, D.S.; Serna-Angel, A.; Ahmad, S.; Azuelos, G.; Bertl, W.; Blecher, M.; Chen, C.Q.; Depommier, P.; von Egidy, T.; Gorringer, T.P.; Hasinoff, M.D.; Henderson, R.S.; Larabee, A.J.; Macdonald, J.A.; McDonald, S.C.; Poutissou, J.M.; Poutissou, R.; Robertson, B.C.; Sample, D.G.; Taylor, G.N.; Wright, D.H.; Zhang, N.S. Radiative muon capture on Al, Si, Ca, Mo, Sn, and Pb. *Phys. Rev. C* **1992**, *46*, 1094–1107. doi:10.1103/PhysRevC.46.1094.
45. Bergbusch, P.C. Radiative muon capture of oxygen, aluminum, silicon, titanium, zirconium, and silver. PhD thesis, University of British Columbia, 1995. doi:<http://dx.doi.org/10.14288/1.0085124>.
46. Gorringer, T.P.; Armstrong, D.S.; Chen, C.Q.; Christy, E.; Doyle, B.C.; Gumplinger, P.; Fearing, H.W.; Hasinoff, M.D.; Kovash, M.A.; Wright, D.H. Isotope dependence of radiative muon capture on the $^{58,60,62}\text{Ni}$ isotopes. *Phys. Rev. C* **1998**, *58*, 1767–1776. doi:10.1103/PhysRevC.58.1767.
47. Rood, H.; Tolhoek, H. The theory of muon capture by complex nuclei: (III). Radiative muon capture. *Nuclear Physics* **1965**, *70*, 658–692. doi:[https://doi.org/10.1016/0029-5582\(65\)90463-3](https://doi.org/10.1016/0029-5582(65)90463-3).
48. Christillin, P.; Rosa-Clot, M.; Servadio, S. Radiative muon capture in medium-heavy nuclei. *Nuclear Physics A* **1980**, *345*, 331–366. doi:[https://doi.org/10.1016/0375-9474\(80\)90344-9](https://doi.org/10.1016/0375-9474(80)90344-9).
49. Fearing, H.W.; Walker, G.E. Radiative muon capture in a relativistic mean field theory: Fermi gas model. *Phys. Rev. C* **1989**, *39*, 2349–2355. doi:10.1103/PhysRevC.39.2349.
50. Fearing, H.W.; Welsh, M.S. Radiative muon capture in medium heavy nuclei in a relativistic mean field theory model. *Phys. Rev. C* **1992**, *46*, 2077–2089. doi:10.1103/PhysRevC.46.2077.
51. Bernstein, R.H.; Borrel, L.; Calibbi, L.; Czarnecki, A.; Davidson, S.; Echenard, B.; Heeck, J.; Hitlin, D.G.; Marciano, W.; Middleton, S.C.; Pronskikh, V.S.; Szafron, R. Theory challenges and opportunities of Mu2e-II: Letter of Interest for Snowmass 2021, 2021, [[RF5_RF0-TF6_TF0](https://arxiv.org/abs/hep-ph/2105.00000)].
52. Kitano, R.; Koike, M.; Okada, Y. Detailed calculation of lepton flavor violating muon-electron conversion rate for various nuclei. *Phys. Rev. D* **2002**, *66*, 096002. doi:10.1103/PhysRevD.66.096002.
53. Cirigliano, V.; Kitano, R.; Okada, Y.; Tuzon, P. Model discriminating power of $\mu \rightarrow e$ conversion in nuclei. *Phys. Rev. D* **2009**, *80*, 013002. doi:10.1103/PhysRevD.80.013002.
54. Mohr, P.J.; Newell, D.B.; Taylor, B.N. CODATA recommended values of the fundamental physical constants: 2014. *Rev. Mod. Phys.* **2016**, *88*, 035009. doi:10.1103/RevModPhys.88.035009.
55. Czarnecki, A.; Garcia i Tormo, X.; Marciano, W.J. Muon decay in orbit: Spectrum of high-energy electrons. *Phys. Rev. D* **2011**, *84*, 013006. doi:10.1103/PhysRevD.84.013006.
56. Wang, M.; Audi, G.; Kondev, F.G.; Huang, W.; Naimi, S.; Xu, X. The AME2016 atomic mass evaluation (II). Tables, graphs and references. *Chinese Physics C* **2017**, *41*, 030003. doi:10.1088/1674-1137/41/3/030003.
57. Suzuki, T.; Measday, D.F.; Roalsvig, J.P. Total nuclear capture rates for negative muons. *Phys. Rev. C* **1987**, *35*, 2212–2224. doi:10.1103/PhysRevC.35.2212.